Materials Science and Engineering A 546 (2012) 103–110

Contents lists available at SciVerse ScienceDirect

Materials Science and Engineering A

journal homepage: www.elsevier.com/locate/msea

Phase stability, microstructure and mechanical properties of Li containing Mg-based bulk metallic glass composites

J.D. Plummer[a,b,*], I.A. Figueroa[b,c], I. Todd[b]

[a] Department of Materials, Royal School of Mines, Imperial College London, Prince Consort Road, SW7 2BP, UK
[b] Department of Materials Science and Engineering, University of Sheffield, Mappin Street, Sheffield, S1 3JD, UK
[c] Instituto de Investigaciones en Materiales, Universidad Nacional Autonoma de Mexico, 04510 México D.F., Mexico

ARTICLE INFO

Article history:
Received 4 July 2011
Received in revised form 24 February 2012
Accepted 9 March 2012
Available online 21 March 2012

Keywords:
Bulk amorphous alloys
Composites
Mechanical characterization
Nanoindentation

ABSTRACT

5–15 at.% Li was substituted into a glass forming Mg–Cu–Gd alloy and the effect on glass forming ability, phase development and mechanical properties were studied. Li was found to have a negative impact on glass forming ability, evident from a reduction in the critical diameter. This resulted from a strong tendency to precipitate the body centered cubic (bcc) Mg_7Li_3 phase. The substitution of Li in amounts less than or equal to 9 at.% promoted a two phase glass matrix-bcc crystal composite. Yielding and work hardening were enhanced by raising the amount of Li, causing a maximum plastic strain of approximately 1.6% for 15 at.% Li, attributed to the presence of the bcc crystals. Deformation response is analyzed within the framework of: (1) a need to match microstructure length scales, and (2) a reduced shear modulus in the crystalline phase, as compared to the matrix. A particular focus of this study was thus to consider both the length scale and modulus mismatch ideas applied to composite bulk metallic glasses by Hofmann et al. (Nat. Lett., 2008, 451, 1085–1089) and whether they can explain the large plasticity that Li containing Mg-based alloys have previously displayed. While a comparison of the alloys reported here with those in the literature suggests that the first of these constraints may be being met, deformation is concentrated within the crystalline phase rather than being shear band mediated. The activation energy for dislocation propagation within the ductile precipitates may be lower than for shear transformation zone nucleation in the matrix therefore, providing a constraint for the future design of tough glass matrix composites.

1. Introduction

Bulk metallic glasses (BMGs) are a novel group of alloy that display no long range atomic periodicity, affording them large elastic strains, high yield strengths and an ability to resist chemical attack [1–3]. Indeed, a Pd-based BMG has demonstrated a combination of yield strength and toughness above that of any other engineered metallic system [4]. These encouraging properties are not universal to all BMGs however, with there being the suggestion that alloys with a low kinetic glass fragility index, *m* (i.e. "strong" glass formers) and a combination of elastic properties that may signify large bonding angularity, are intrinsically brittle [5]. Such alloys often include those based on Ce, La, Fe and Mg. In many instances however it has been demonstrated that a two-phase composite microstructure can effectively enhance strain to failure via the interaction of shear bands, nucleated from a shear transformation zone (STZ), in an amorphous phase with crystalline regions that have different elastic properties to the glass [6–11]. Examples of this have been exhibited in La- and Mg-based alloys [6,8–10], where greater plasticity in compression was found over similar monolithic BMGs. A Zr-based BMG composite has been developed which Exhibits 8% ductility in tension, whilst retaining a high yield strength (1.5 GPa) [7]. These properties were considered to result from the formation of body centered cubic (bcc) dendrites frozen into the structure during processing from the semi-solid state. Hexagonal close packed (hcp) dendrites were also found to promote tensile ductility in an as-cast La-based BMG composite [6]. Ductile crystals in a glass matrix can therefore be beneficial in enhancing plastic strain in tension.

The precipitation of bcc dendrites in Mg–Cu–Y BMGs has been demonstrated by substituting Li into the system, leading to plastic strains in excess of 20% [12–14]. This was ascribed mostly to interactions within the multi-phase microstructure and so was not solely facilitated by the presence of the bcc phase – the largest plastic strains were realized with increasing Li content, which destabilized the glassy phase and resultantly malleable crystalline

* Corresponding author at: Department of Materials, Royal School of Mines, Imperial College London, Prince Consort Road, SW7 2BP, UK. Tel.: +44 (0)20 7589 5111; fax: +44 (0) 20 7594 5017.
E-mail address: j.plummer@imperial.ac.uk (J.D. Plummer).

0921-5093/$ – see front matter © 2012 Elsevier B.V. All rights reserved.
doi:10.1016/j.msea.2012.03.034

alloys. In this study we only consider the effect that small Li alloying additions, of up to 15 at.%, have on the glass forming ability (GFA), structure and compressive mechanical properties of $Mg_{61}Cu_{28}Gd_{11}$. This base composition was selected because it has a critical diameter (the largest section size over which an amorphous rod can be cast) of 12 mm [15]. Only small amounts of Li are studied here so to understand the role that the bcc phase alone plays in mechanical deformation in the glass composite. Through this, we aim to understand the effect that bcc crystallites alone can have on room temperature mechanical properties by considering the analysis of Hoffmann et al. [7], with regard to (1) matching of microstructure length scales, and (2) small shear modulus mismatch. The analysis presented and the conclusions that are drawn are believed to have implications for the development of BMG composites, irrespective of composition.

2. Experimental procedure

Alloys with nominal composition $(Mg_{0.61}Cu_{0.28}Gd_{0.11})_{100-x}Li_x$ (x = 0, 5, 7, 9, 11, 13 and 15) were weighed out from high purity elements (≥99.8%). Master alloys of Cu–Gd were prepared by arc melting in an atmosphere evacuated to 5×10^{-3} Pa and backfilled with 1/3 atmosphere of argon. A Ti "getter" was employed to remove residual oxygen during melting and ingots were inverted and melted three times and were subsequently broken up and placed in boron nitride crucibles. Mg and Li were added to the crucibles and placed inside of a vacuum induction melter with an excess of 5 at.% Mg and Li so as to balance evaporation losses during melting. It should be noted that the Li used in alloy manufacture was stored in mineral oil and the time between weighing out, de-greasing with isopropanol and placing in the vacuum induction melter was minimized in order to prevent oxide formation. The alloy was induction melted twice (chamber evacuated to 5×10^{-3} Pa) under flowing argon with the melt being agitated during production, and was broken up between melts to encourage homogenization. Rods with a diameter of 2.5 mm and a length of 40 mm were prepared by injection casting from a quartz crucible into a copper die by the application of an argon over-pressure, within a vacuum chamber evacuated to 5×10^{-3} Pa and backfilled with 2/3 atmosphere of high purity argon.

X-ray diffraction (XRD) was performed on a Phillips PW1825 on the cross-section of each alloy at a slow scan rate of 0.02 2θ per second. A Perkin Elmer Diamond DSC was used for Differential Scanning Calorimetry (DSC), in alumina pans with a heating rate of 30 K/min up to 800 K, with a sample mass of 20 mg. Samples for scanning electron microscopy (SEM) were polished to a mirror finish and were examined using a JEOL 6400 and an FEI Inspect F FEG SEM. Samples for quasi-static compression testing were polished to create parallel surfaces with a rod aspect ratio of 2:1 and testing was performed on a Hounsfield testing device with a compliance reading taken and subsequently subtracted from the data, resulting in the real deformation response. At least six samples were tested for each composition to ensure reproducibility of results. A Hysitron Nanomechanical tester (coupled to a scanning probe microscope) fitted with a Berkovitch diamond tip was used to indent specific phases within the composite microstructure. Two loads were applied (3 and 5 mN) for the characterization of each phase, and 5 different regions were probed for each phase and applied load. Indentation was performed within the centre of large phase regions, so to minimize the contribution to the resulting data from surrounding phases. The load, hold and unload regions of the loading schedule each had segment times of 5 s.

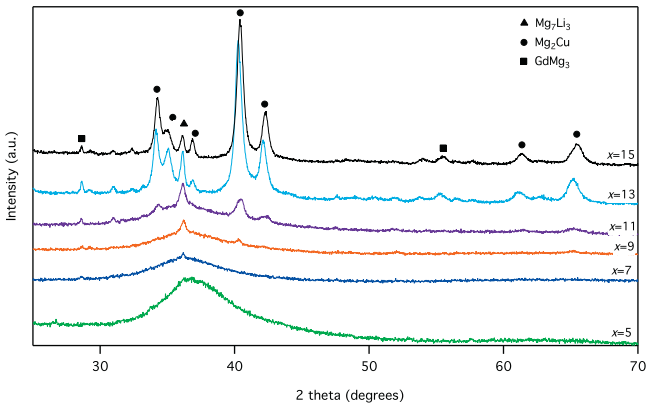

Fig. 1. XRD traces for alloys in the $(Mg_{0.61}Cu_{0.28}Gd_{0.11})_{100-x}Li_x$ series.

3. Results and discussion

3.1. Glass formation and phase stability

Fig. 1 presents XRD traces for alloys in the x = 5 to x = 15 alloy series where x is the atomic percent of Li added to the base $Mg_{61}Cu_{28}Gd_{11}$ alloy. The substitution of 5 at.% Mg results in a structure with no long range order, within the limits of the XRD technique, resulting in a broad amorphous peak between 30 and 50 2θ. Since this composition could be cast with a fully amorphous structure that exceeded 1 mm in the smallest dimension, it can be considered a bulk glass former. The trace for the x = 7 alloy contains a slight peak which is suggestive of the formation of crystals and, as the amount of Li is further raised, the intensity of this peak increases proportionately. It has been reported in the literature that bcc Mg_7Li_3 is the first phase to precipitate from the glass when Li was substituted into $Mg_{65}Cu_{25}Y_{10}$ [12]; phase identification software (Win X Pow version 2.10) on the peak for the x = 7 alloy identifies that these are the first crystals to form in the Mg–Cu–Gd–Li system also. The intensity of this characteristic peak strengthens with Li content, suggesting the formation of an increased amount of the bcc phase, though the intermetallic Mg_2Cu (orthorhombic crystal structure) phase appears to become the dominant crystalline phase as Li content is raised further.

DSC data for x = 0 to x = 15 alloys can be seen in Fig. 2 and characteristic temperatures are collected in Table 1. The base alloy (x = 0) displays a defined glass transition and single crystallization and melting events. The fully amorphous (x = 5) Li containing alloy shows an initial exothermic event prior to the main crystallization peak. As Fig. 1 suggests that Mg_7Li_3 precipitates ahead of others it can be expected that this peak correlates to this. The area under the initial exothermic peak also appears to decrease with Li content as there is more Li in the amorphous phase when the value of x is low and so more Li is available to precipitate out and form Mg_7Li_3 during thermal analysis. In x = 15 there are no observable glass or crystallization transitions, suggesting that the structure is fully crystalline. The temperature range of the melting process

Table 1
Thermal transition temperatures and measures of glass formation for alloys in the $(Mg_{0.61}Cu_{0.28}Gd_{0.11})_{100-x}Li_x$ series.

Alloy	T_g (K)	T_x (K)	T_s (K)	T_l (K)	T_{rg}	ΔT_x	γ
x = 0	425	489	671	709	0.60	64	0.43
x = 5	404	430	649	703	0.57	26	0.39
x = 7	404	425	653	719	–	–	–
x = 9	419	469	652	727	–	–	–
x = 11	424	473	649	734	–	–	–
x = 13	419	472	650	756	–	–	–
x = 15	–	–	651	770	–	–	–

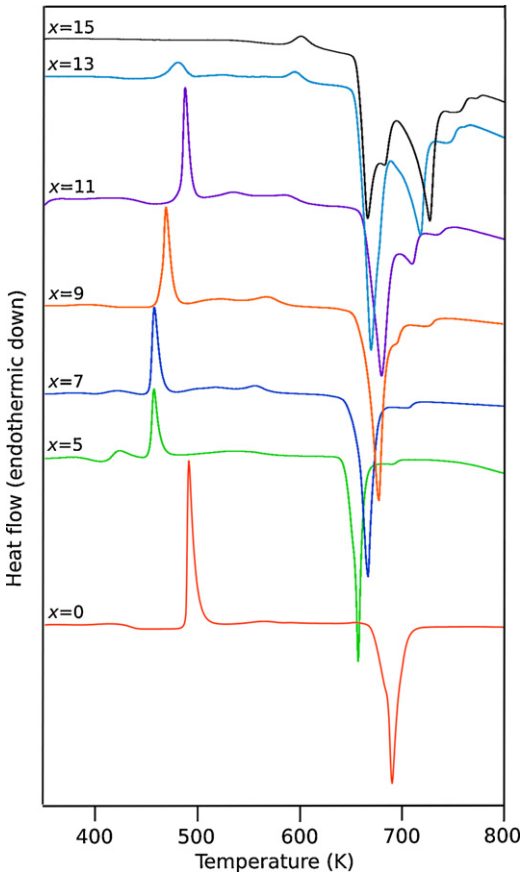

Fig. 2. DSC data for $(Mg_{0.61}Cu_{0.28}Gd_{0.11})_{100-x}Li_x$ alloys.

(between the solidus temperature, T_s, and liquidus temperature, T_l) increases with x, with the process exhibiting a more complex melting of multiple phases, suggesting a less homogeneous structure than in alloys containing less Li.

Thermal parameters often used to quantify GFA, including T_{rg} ($T_{rg} = T_g/T_l$), ΔT_x ($\Delta T_x = T_x - T_g$) and γ ($\gamma = T_x/(T_g + T_l)$), are presented for $x = 0$ and $x = 5$ alloys in Table 1, where T_g and T_x are the glass transition and crystallization temperatures respectively. They all show a clear reduction in the $x = 5$ bulk glass former in comparison to the base ternary alloy. This may originate from poor thermal stability (low T_g) of the amorphous phase and the concomitantly low T_x as a result of the large thermodynamic driving force for the precipitation of bcc crystals when in the presence of Li. Both T_g and T_x increase up to values similar to that of the base alloy in the $x = 9$, $x = 11$ and $x = 13$ alloys, indicating that a substantial portion of Li has partitioned to Mg_7Li_3 during casting, and so less remains in the amorphous phase to precipitate during DSC. The presence of Li in the glassy phase of Mg-based alloys therefore prevents large diameter glassy castings, resulting from its poor thermal stability and tendency to precipitate a bcc phase.

3.2. Microstructure and deformation behaviour

To characterize microstructure development with increasing Li at.%, SEM micrographs were taken and can be seen in Figs. 3 and 4, where regions of specific interest have been labelled. It is apparent that crystallites have nucleated in the $x = 7$ alloy and comparison of Figs. 1 and 3a suggests that these are the bcc Mg_7Li_3 phase and that their size increases with Li content. Their volume faction, V_f, was determined using Carl Zeiss KSRUN Version 3.0 software and the results are given in Table 2. V_f increases with Li content in the $x = 7$ and $x = 9$ alloys from 12% to 21%, accounting for the increased intensity of the Mg_7Li_3 peak in the XRD traces. For $x = 11$ and $x = 13$ the microstructure visibly contains a large number of dendrites and multiple phases, as the XRD data in Fig. 1 suggest. This accounts for the multistage melting phenomena observed in the DSC scans. In Fig. 4b Mg_2Cu preferentially nucleates around the bcc phase, presumably as a result of a lower interfacial energy. This may explain the apparent similar V_f of the bcc phase in the $x = 13$ and $x = 15$ alloys since the presence of these crystals act as nucleation sites, constraining further growth, and so an upper limit on V_f of approximately 40% may be being imposed.

Representative quasi-static room temperature compressive stress–strain curves are presented in Fig. 5, with the data collated in Table 2. The mechanical data collected in this data represents an average of at least 6 samples tested for each composition, with the maximum and minimum values also being reported in Table 2. From these tables the following trends may be observed: (1) the amount of elastic strain and yield point both decrease with increasing values of x, (2) the amount of plastic strain accommodation increases with x, and (3) the failure strength is approximately constant for all Li containing alloys. To consider these observations it is pertinent to use ideas relating to the formation of toughened partially devitrified glass–crystal composites [7], since Figs. 3 and 5 suggest that this may be the source of plasticity here. It has been shown that the presence of a deformable crystalline phase within an amorphous matrix can effectively blunt the propagation of a shear band, leading to stress concentration and STZ formation in another energetically favourable region [6,7,11]. Elastic instability around the soft (lower shear modulus, G) crystalline phase also promotes shear banding via a reduction in STZ activation energy [7]. By these mechanisms, multiple shear banding is possible, allowing for large plastic strain accumulation. The matching of microstructure length scales, with respect to plastic zone size, r_p, and separation distance between bcc dendrites (with a lower G than the matrix), in a composite derived from a Zr-based BMG, was cited as being another determining feature as to whether large plasticity in tension would be observed [7]. In this reference, r_p and dendrite separation distance were reported to be 200 μm and 80–140 μm respectively and so shear bands within the amorphous region did not reach instability. Applying such ideas to Mg-based BMGs, r_p can

Table 2
Mechanical, properties for $(Mg_{0.61}Cu_{0.28}Gd_{0.11})_{100-x}Li_x$ alloys. σ_y, σ_f, ε_e, ε_p and V_f are the yield point, failure strength, elastic strain, plastic strain and volume fraction respectively. The average (Avg) of at least six alloys tested for each composition are reported, as well as the maximum (Max) and minimum (Min) values.

Alloy	σ_y (GPa)			σ_f (GPa)			ε_e (%)			ε_p (%)			V_f Mg_7Li_3 (%)
	Avg	Max	Min	Avg	Max	Min	Avg	Max	Min	Avg	Max	Min	
$x = 0$	–	–	–	0.77	0.77	0.75	1.67	1.70	1.51	0	0	0	–
$x = 5$	–	–	–	0.64	0.67	0.61	1.51	1.54	1.48	0	0	0	0
$x = 7$	–	–	–	0.65	0.68	0.62	1.66	1.67	1.64	0	0	0	12
$x = 9$	0.60	0.62	0.56	0.63	0.67	0.59	1.57	1.81	1.49	0.10	0.25	0.06	21
$x = 11$	0.53	0.57	0.49	0.69	0.70	0.67	1.45	1.40	1.49	0.53	0.57	0.41	32
$x = 13$	0.40	0.42	0.35	0.65	0.67	0.62	1.16	1.25	1.12	0.91	0.82	1.35	38
$x = 15$	0.38	0.42	0.36	0.64	0.65	0.60	0.94	1.26	0.90	1.59	1.63	1.49	40

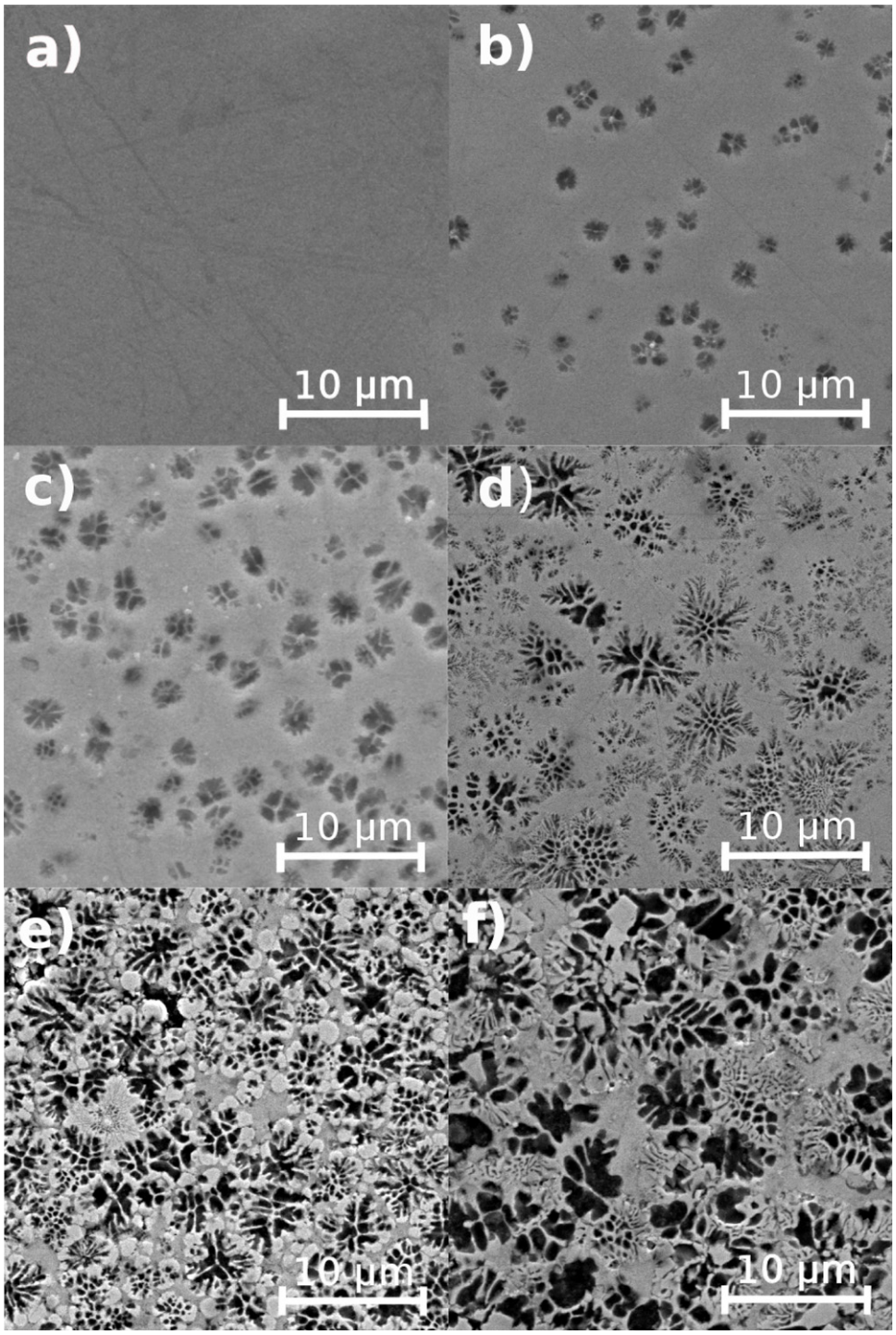

Fig. 3. Micrographs of $(Mg_{0.61}Cu_{0.28}Gd_{0.11})_{100-x}Li_x$ alloys, where $x = 5$, 7, 9, 11, 13 and 15 for (a)–(f) respectively.

be calculated from Eq. (1) [16], where K_{1C} is the fracture toughness, G the shear modulus and γ_c the critical shear strain (=0.0267) [17]:

$$r_p = \frac{K_{1C}^2}{8\pi G^2 \gamma_c^2} \quad (1)$$

Using reported values for K_{1C} and G for $Mg_{65}Cu_{25}Gd_{10}$ of 0.72 MPa $m^{1/2}$ [18] and 18.6 GPa [17] respectively, an r_p of 84 nm results, with a value of 580 nm for $Mg_{65}Cu_{25}Tb_{10}$ (K_{1C} and G of 2 MPa $m^{1/2}$ and 19.6 GPa respectively [19]). Mg-based BMGs have a tendency to fail in a brittle manner, typically without yielding, as a result of their high G/B ratio [19] and because of there being a strong directional nature to interatomic bonding, preventing stable re-arrangement under an applied load [5]. K_{1C} is therefore seen to be typically limited, resulting in the small plastic zone sizes determined here. Table 3 collects data for two phase glass composites from the literature which have been produced by precipitation of a crystalline phase rather than by particle inclusion, and which show large plastic strain in either uniaxial compression and/or tension. The $x = 9$ two phase alloy reported here is also included to permit a comparison. The r_p of the matrix (determined from data for monolithic BMGs with similar compositions) and the average

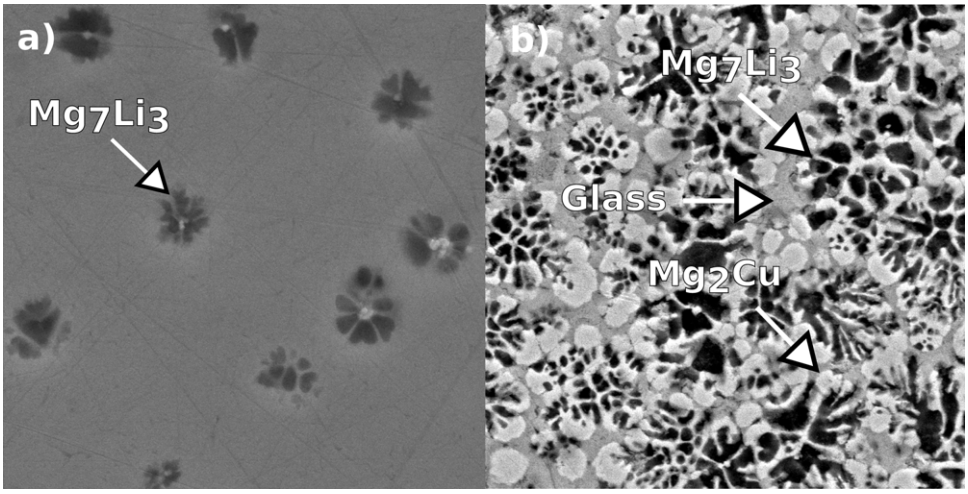

Fig. 4. Micrographs of $x = 7$ (a) and $x = 13$ (b) alloys.

Table 3
Mechanical properties (ε_p, plastic strain and G, shear modulus) and microstructure parameters (V_f, volume fraction, r_p, plastic zone size and S, average intercrystal separation distance) for two-phase glass matrix composites from the literature and in this study. Note (C) and (G) represent the crystalline and glass phase respectively.

Alloy	ε_p (%)	V_f (%)	r_p (μm)	S (μm)	(r_p/S)	G (GPa)	ΔG (GPa)	Ref.
$Zr_{36.6}Ti_{31.4}Nb_7Cu_{5.9}Be_{19.1}$ (DH1)	7.6[a]				2.2			[7]
$Zr_{40-44}Ti_{42-45}Nb_{11-14}Cu_{1-3}$ (C)		42		112		28.7	4.5	
$Zr_{31-34}Ti_{17-22}Nb_{1-2}Be_{31-38}$ (G)		58	250			33.2		
$La_{74}Al_{14}Cu_6Ni_6$	5[a], 4.1[b]				1×10^{-5}			[5,6,23]
La (C)		50		10		14.9	1.5	
$La_{66}Al_{14}Cu_{10}Ni_{10}$ (G)		50	1×10^{-4}			13.4		
$Mg_{81}Cu_{9.3}Y_{4.7}Zn_5$	18.5[b]				0.01			[9,22,23]
Mg (C)		48		7		17.3	2.3	
$Mg_{65}Cu_{25}Y_{10}$ (G)		52	0.08			19.6		
$Mg_{55.5}Cu_{25.5}Gd_{10}Li_9$	0.1[b]				0.01			[17,24]
$Mg_{6.5}Li_{3.5}$ (C)		21		6		7.3[c]	11.3	
$Mg_{65}Cu_{25}Gd_{10}$ (G)		79	0.08			18.6		

[a] Value from tensile testing.
[b] Value from compression testing.
[c] Theoretical value determined at 0 K.

interparticle separation distance, S, have been calculated for each alloy. r_p was determined from Eq. (1) and S from Eq. (2) [25], where r is the average crystal radius:

$$S = 1.23r\left(\frac{2\pi}{3V_f}\right)^{1/2} \quad (2)$$

Eq. (2) assumes a spherical particle radius, which is not always the situation in the alloys in Table 3 (precipitates in [6] and [9] have high aspect ratios) and so the average particle radius is used in these calculations. By using this method, S is determined in a consistent manner and so enables a fairer comparison between alloy systems. In Table 3, an S value of approximately 6 μm was determined for $x = 9$, which would appear realistic based on the micrograph in Fig. 3c. It is apparent that for all the alloys apart from DH1 [7], r_p is less than S (i.e. $r_p/S < 1$) and so the earlier reported criteria are not being met despite the observation of large strain accumulation. It should be noted that as the bcc crystals act as nucleation sites for further devitrification to the orthorhombic phase, appearing to limit V_f of the bcc phase to 40%, it is not possible to increase the amount of Mg_7Li_3 in the microstructure without precipitating other phases also and so the technique of matching plastic zone size to crystal separation distances is unlikely to work in this alloy series. However, Lee et al. consider it to be the shear band separation distance that must be matched by the scale of the microstructure in order to constrain shear bands, hence preventing them from becoming unstable [6]. This is generally much larger than r_p in brittle alloys because r_p is so small. The separation distances of bcc Mg_7Li_3 in the two-phase (glass matrix-bcc precipitates) $x = 7$ and $x = 9$ alloys have values of 8 μm and 6 μm respectively (from Eq. (2)), which far exceed r_p (approximately 84 nm from Eq. (1)). However the value of r_p/S are greater than, or comparable to, the toughened La- and Mg-based composites and so the scale of the microstructure may be suitable for plastic strain accumulation if it is shear band spacing that is critical. Thus it would appear that a matching of microstructure length scales is not the only

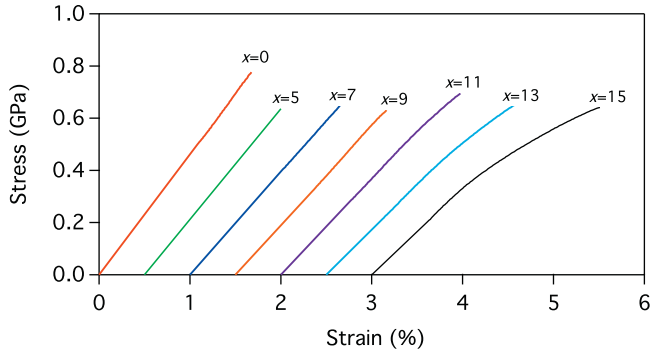

Fig. 5. Quasi-static compression stress–strain curves for $(Mg_{0.61}Cu_{0.28}Gd_{0.11})_{100-x}Li_x$ alloys.

Table 4
Nanoindentation results when indenting the glassy matrix of $x = 7$ and the bcc phase of $x = 15$, at loads of 3 and 5 mN.

Indent	H_v-matrix (GPa)		H_v-bcc (GPa)		E_r-matrix (GPa)		E_r-bcc (GPa)	
	3 mN	5 mN	3 mN	5 mN	3 mN	5 mN	3 mN	5 mN
1	3.59	3.41	1.75	1.69	69.2	69.2	53.7	51.5
2	3.57	3.46	1.78	1.73	68.5	64.8	51.6	50.9
3	3.49	3.63	1.81	1.78	66.4	71.4	50.6	52.4
4	3.55	3.70	1.80	1.77	70.1	65.6	52.5	54.9
5	3.60	3.30	1.76	1.73	68.8	69.0	55.6	50.8
Average	3.56	3.50	1.78	1.74	68.6	68.0	52.8	52.1

critical factor in developing large plastic strains in these composites. It should be mentioned that multiple length scales are concurrently involved in deformation (ranging from STZs on the atomic scale up to precipitates on the micron scale and even potential macroscopic percolation, believed to occur when $V_f \approx 40\%$ [6]) and so a complex interplay between them may exist. Also, three unique regions are present: (1) the matrix, (2) the crystals, and (3) the interface. These will all respond differently to a mechanical stimulus, coupled with the likelihood of load partitioning between them, and so understanding the mechanisms of plasticity in composites is a complex, multi variable issue.

Although the length scales of the microstructure may be suitable for shear band mediated deformation, plastic strain reaches a maximum in the $x = 15$ alloy, with an average of 1.59%, which is much lower than the other alloys in Table 3. However, controlled devitrification of $Mg_{65}Cu_{25}Gd_{10}$, to crystalline volume fractions between 0% and 100%, caused an embrittling of the alloy, with the failure strength decreasing and no yield event taking place in any of the alloys, including the BMG [20]. The XRD and DSC data in Figs. 1 and 2, respectively, suggest that Li promotes bcc phase formation, and so this is the major structural difference between Mg–Cu–Gd alloys that contain Li to those that do not. Therefore, it is Mg_7Li_3 that is permitting some plastic strain in these alloys. When plasticity occurs in BMGs, where it is accommodated via STZ formation and shear banding, serrations are typically observed in the plastic regime, with the absence of strain hardening [21]. In Fig. 5 no serrations are visible in the plastic regions and strain hardening is seen. This implies that dislocation movement and interactions within Mg_7Li_3 are the source of yielding and plastic strain – this conclusion was reached in [14], where the specific details of the failure mechanisms of these alloys were studied. Table 2 suggests a critical V_f of approximately 21% for macroscopic yielding to be detected. More will be committed on deformation mechanisms next.

As previously mentioned, it has been reported that an elastically soft crystalline phase in an amorphous matrix can encourage shear banding as the low G crystals create elastic instability around the amorphous matrix [7]. It would be anticipated that G of the bcc crystals studied here may be lower than that of the matrix as the crystals are composed of Mg and Li, which have a low G of 17.3 GPa and 4.2 GPa respectively, in comparison to Cu and Gd (48.3 GPa and 20.8 GPa respectively) (G values from [23]), which are found in the matrix in these alloys. Nanoindentation was used to study the mechanical properties of the glass matrix and Mg_7Li_3 independently, by indenting the glass matrix in $x = 7$ and large Mg_7Li_3 crystals in $x = 15$. It should be noted that the composition of the glass matrix will vary slightly in each sample, as the amorphous phase is steadily destabilized as Li content increases, though the extent of chemical variation will be limited. A measure of the Young's modulus, E, termed the reduced modulus, E_r, is obtained from the nanoindentation test, though it cannot be considered comparable to E as there is an elastic contribution from the indenter also. The results of this study are visible in Table 4. When considering this data it should be noted that some effect from the surrounding phases is likely to influence the recorded data. Using lower loads reduces indent size, limiting the size of the strain field around the indent and therefore reducing any contribution from the surroundings. However, applying lower loads can equally impose problems, associated with inaccuracy caused by greater sensitivity to surface roughness and the need for a sharp Berkovitch indenter tip and an accurate tip area function [26,27]. Probing the mechanical properties of thin layers is thus a non-trivial task [27]. For the data in Table 4 however, spread in the data is within a reasonably narrow limit, suggesting that the above factors are at least approximately equivalent for each indent. Using this technique, the average hardness, H_v, and E_r of the glass matrix and crystals were measured as 3.50 GPa and 68.0 GPa, and 1.74 GPa and 52.1 GPa respectively when using an applied load of 5 mN, and 3.7 GPa and 70.2 GPa, and 1.78 and 55.1 GPa for a load of 3 mN. Mg_7Li_3 is therefore significantly softer than the matrix, both physically and elastically. Due to the afore mentioned issues with nanoindentation, the actual size of the numbers is essentially unimportant; it is their value relative to one another that is most pertinent to these discussions. E is known to scale with G [16], and so variation in E_r will be mirrored in G. Extraction of E from E_r requires knowledge of Poisson's ratio of the indented phases, which cannot be accurately verified in this instance. The link between E scaling with G in metals (and which has specifically been shown in BMGs [16]) has long been known however [28] and so it can be assumed that a low E_r will result in low G. Given the significantly lower G of the bcc crystals, rather than them promoting shear band nucleation around the interface, yielding may occur by dislocation activation as G is significantly lower in Mg_7Li_3. It should be mentioned at this point that Gonzalez et al. have considered in detail the mechanism of plasticity in a Mg–Cu–Y–Li alloy which showed near identical mechanical characteristics to those shown in Fig. 5 for small plastic strains, via a microscopy analysis [14]. In this study, up to 2% plastic strain was found to be accommodated by dislocation slip in the bcc phase, after which micro-cracks started to form, which could subsequently be blunted by the bcc phase. Fig. 5 and Table 2 similarly suggest approximately 2% strain hardening and, given their compositions both being Mg–Cu–RE–Li (RE = a rare earth element), it is reasonable to conclude that dislocation activity in the bcc phase is responsible for work hardening in the alloys studied here also. Moreover, BMGs are known to work soften and so the amorphous phase cannot be the source of work hardening, while intermetallic phases are generally brittle, which were indeed shown to be sites for micro-cracks by Gonzalez et al. Given this result, for the toughening mechanism described in [7] to take effect, as well as the need for a matching of microstructural length scales, G may be required to be only slightly lower than the matrix otherwise dislocation movement will accommodate the applied mechanical stimulus, as the activation energy for nucleation of a shear transformation zone is not reached.

To consider this hypothesis in more detail, Table 3 presents data for the difference in G between glass and crystalline phases (ΔG). It is apparent that in all situations apart from the alloys developed here, ΔG between crystal and matrix is limited to a maximum of

4.5 GPa, in comparison to the brittle $x = 9$ alloy, which exhibited a ΔG of 11.3 GPa. The value for $Mg_{6.5}Li_{3.5}$ was determined at 0 K and from theoretical values, with an error margin of approximately 8% [24]. As elastic moduli decrease with increasing temperature, this value represents a maximum and so ΔG may in fact be much larger than the value suggested here. Two points must be noted when studying this data: (1) in all cases apart from [7] (the DH1 alloy), G is determined from values for similar compositions in the available literature and so ΔG should only be considered an estimate, and (2) V_f of the crystalline phase in the $x = 9$ composite reported in this study (21%) is less than that of the other systems (including $x = 13$), where V_f is approximately 50%. For the La-based composite the values in Table 3 would suggest that G is larger in the crystal than in the matrix. However this difference is small (0.9 GPa) and the first limitation mentioned here may account for this. Despite these issues we would suggest that a definite trend does exist in Table 3 and so the magnitude of ΔG should be taken into account when designing glass matrix composites, as if the difference is too great the activation barrier for STZ nucleation will not be reached and dislocation motion within the ductile phase may occur in preference.

Evaluating the activation energies for (1) STZ nucleation and propagation, and (2) dislocation propagation, is non-trivial and so limited experimental attempts to resolve the activation energy for STZs exist. Puthoff et al. [29] suggest experimentally determined values of 480–965 kJ/mol in ternary Zr–Cu–Al BMGs, while Chang et al. [30] suggest values of 113 kJ/mol in $Mg_{65}Cu_{25}Gd_{10}$ and 316 kJ/mol in $Mg_{65}Cu_{22}B_3Gd_{10}$. bcc Mg–Li is known to be a highly ductile phase however, and the activation energy for dislocation glide in a two phase hcp–bcc Mg–9.5 wt% Li–1.0 wt% Zn alloy was determined as 92 kJ/mol [31], and so significantly less than many of the estimates for STZs. Moreover, Metenier et al. [32] report that the activation of self diffusion in low valence bcc metals can be approximated to $14.3RT_m$, where R is the gas constant and T_m the melting point. For the alloys studied here, assuming a T_m of 700 K (it is difficult to exactly verify T_m due to the multistage melting events visible in Fig. 2), an activation energy for self diffusion of 83 kJ/mol results. This concurrently suggests ease of dislocation movement, in comparison to STZ nucleation.

On a qualitative level the importance of G in determining activation energy in amorphous and crystalline metals is clear; the activation energy for STZ nucleation is proportional to GV (where V is the sheared volume) in both the shoving model [33] and in the cooperative shear model [17], while the force required to propagate a dislocation is proportional to Gb, where b is the burgers vector. It is justifiable to assume that a large dislocation content is present in the bcc crystals, since their size is significantly greater than in systems that have been shown to approach theoretical strength ($0.1G$) [34] (e.g. in nanopillars and whiskers), where dislocations have to be nucleated first. It can be assumed then that it is the Peierls–Nabarro force that must be overcome for plastic flow to proceed. While no simple equivalency between V in BMGs and b in crystalline metals exists, the significance of G in controlling plastic yielding is clear. The lower G of the bcc phase determined here by nanoindentation therefore provides strong evidence that plastic yielding occurs there first, rather than by STZ nucleation in the glass matrix.

Though the alloys reported here exhibit limited failure strains, by increasing the Li content in the Mg–Cu–Y–Li alloy system to 19 at.%, 25% plastic strain in compression was measured [13,14]. As mentioned earlier, less than 2% was found to be accommodated by work hardening of the Mg–Li containing phase and this is in broad agreement with the $x = 15$ alloy showing an average 1.59% plastic strain through strain hardening. While the Mg–Cu–Y–Li system exhibited a load plateau after work hardening, accommodating the majority of the total strain, the alloys investigated in this study fail rather than entering a steady-state regime. The reported reason for large plastic strains in the Y containing alloys was that the bcc and Mg_2Cu phases could blunt microcracks. Given the similarity of the alloy compositions, that the microstructures are dominated by the same phases (bcc Mg–Li and Mg_2Cu) and that the deformation mechanism appears to be the same in the alloys studied here as in [14], it is not immediately apparent why the Y containing alloys are superior plastic deformers to the Gd containing system. One possible explanation is that after work hardening of the Mg–Cu–Y–Li alloys the sample is loaded to around 0.5 GPa, whereas in the Gd containing alloys this value increases to around 0.65 GPa. Additionally, the higher yield point of the Gd alloy (approximately 0.38 GPa compared to 0.275 GPa) means that more elastic energy is being stored. In this higher stress state, microcracks will have a greater energy content and so may be more difficult to blunt. Another possibility is that observed plasticity during the testing of BMGs in compression is very sensitive to machine stiffness [35] and platen lubricant [36]. Reported plasticity between different research groups, using different techniques and operation practice, is likely to vary therefore, and represents a universal issue for the comparison of mechanical data produced on different test rigs.

4. Conclusion

Between 5 at.% and 15 at.% Li was added to a good glass former in the Mg–Cu–Gd system. The presence of Li acted to destabilize the glassy phase, causing poor thermal stability and a high driving force for the preferential precipitation of bcc-Mg_7Li_3, resulting in a fully amorphous structure in rods with a 2.5 mm diameter that contained 5 at.% Li. As Li promotes the nucleation and growth of a bcc phase it was possible to obtain a two-phase glass matrix-bcc crystal composite, and, by varying the Li content, the volume fraction of the bcc phase increased up to an apparent maximum value of approximately 40%, as a result this phase providing a preferential nucleation site for other phases. Whilst plasticity was observed to increase from that of the alloy that contained no Li, this increase was attributed to dislocation motion within the bcc phase and was not mediated by shear banding. In addition, it is suggested that while the scale of the microstructure may be suitable for shear band induced toughening, the relative ease of dislocation propagation in the crystalline phase means that deformation is controlled by dislocations rather than STZs and shear bands. Thus, we suggest that the shear modulus of an elastically soft phase, present as discrete regions within a continuous higher modulus matrix, should be only slightly reduced if elastic instability is to be induced at the interface, thereby creating conditions for shear band mediated deformation. If not, deformation may only be accommodated within the softer phase, severely limiting plastic strain. Finally, an apparent inability for the bcc phase to blunt microcracks prevents the attainment of the large plastic strains that have been found in similar alloys.

Acknowledgements

Technical support provided by P. Hawksworth was gratefully received and A. Cunliffe and M. Lopez-Pedrosa are thanked for SEM assistance. JDP acknowledges a studentship from the Engineering and Physical Sciences Research Council (EPSRC). This work was funded by the Innovative Metal Processing Center (IMPC).

References

[1] C. Schuh, T. Hufnagel, U. Ramamurty, Acta Mater. 55 (2007) 4067.
[2] A. Inoue, Acta Mater. 48 (2000) 279.
[3] W.L. Johnson, MRS Bull. 24 (1999) 42.
[4] M.D. Demetriou, M.E. Launey, G. Garrett, J.P. Scramm, D.C. Hofmann, W.L. Johnson, R.O. Ritchie, Nat. Mater. 10 (2011) 123–128.
[5] J.D. Plummer, I. Todd, Appl. Phys. Lett. 98 (2011) 021907.
[6] M.J. Lee, Y. Li, C.A. Schuh, Acta Mater. 52 (2004) 4121–4131.

[7] D.C. Hofmann, J.Y. Suh, A. Wiest, G. Duan, M.L. Lind, M.D. Demetriou, W.L. Johnson, Nat. Lett. 451 (2008) 1085–1089.
[8] Y.K. Xu, H. Ma, J. Xu, E. Ma, Acta Mater. 53 (2005) 1857–1866.
[9] X. Hui, W. Dong, G.L. Chen, K.F. Yao, Acta Mater. 55 (2007) 907–920.
[10] K.Q. Qui, N.N. Hu, H.B. Zhang, W.H. Jiang, Y.L. Ren, P.K. Liaw, J. Alloys Compd. 478 (2009) 419–422.
[11] F.Q. Guo, S.J. Poon, G.J. Shiflet, Philos. Mag. Lett. 88 (2008) 615–622.
[12] W. Liu, W.L. Johnson, J. Mater. Res. 11 (1996) 2388–2392.
[13] S. Gonzalez, D.V. Louzguine, J.H. Perepezko, A. Inoue, J. Alloys Compd. 504 (2010) 114–116.
[14] S. Gonzalez, D.V. Louzguine, J.H. Perepezko, A. Inoue, Intermetallics 18 (2010) 859–863.
[15] Q. Zheng, S. Cheng, J.H. Strader, E. Ma, J. Xu, Scr. Mater. 56 (2007) 161–164.
[16] J.D. Plummer, R. Goodall, I.A. Figueroa, I. Todd, J. Non-Cryst. Solids 357 (2011) 814–819.
[17] W.L. Johnson, K. Samwer, Phys. Rev. Lett. 95 (2005) 195501.
[18] F. Zhenjun, Z. Zhiyuan, J. Zengbao, Sci China Phys. Mech. Astron. 53 (2010) 654–657.
[19] J.J. Lewandowski, W.H. Wang, A.L. Greer, Philos. Mag. Lett. 85 (2005) 77.
[20] J.L. Soubeyroux, S. Puech, P. Donnadieu, J.J. Blandin, J. Alloys Compd. 434 (2007) 84–87.
[21] H.M. Chen, J.C. Huang, S.X. Song, T.G. Nieh, J.S.C. Jang, Appl. Phys. Lett. 94 (2009) 141914.
[22] M. Jiang, L. Dai, Phys. Rev. B. 76 (2007) 054204.
[23] C. James, Smithells Metals Reference Book, 7th ed., Butterworth Heinemann, Oxford, 1992.
[24] P. Beauchamp, R. Taylor, V. Vitek, J. Phys. F: Metal Phys. 5 (1975) 2017–2025.
[25] A.J.E. Foreman, M.J. Makin, Philos. Mag. 14 (1966) 1911.
[26] D.R. Tadjiev, R.J. Hand, S.A. Hayes, Philos. Mag. 90 (2010) 1819–1832.
[27] D.R. Tadjiev, S.A. Hayes, J. Non-Cryst. Solids 356 (2010) 102–108.
[28] H.M. Ledbetter, Mater. Sci. Eng. 27 (1977) 133–136.
[29] J.B. Puthoff, H.B. Cao, J.E. Jakes, P.M. Voyles, D.S. Stone, Mater. Res. Soc. Symp. Proc. 1152 (2008) TT10-01.
[30] Y.C. Chang, J.C. Huang, Y.T. Cheng, C.J. Lee, X.H. Du, T.G. Nieh, J. Appl. Phys. 103 (2008) 103521.
[31] M. Kawasaki, K. Kubota, K. Higashi, T.G. Langdon, Mater. Sci. Eng. A 429 (2006) 334–340.
[32] P. Metenier, G. Gonzalez-Doncel, O.A. Ruano, J. Wolfenstine, O.D. Sherby, Mater. Sci. Eng. A 125 (1990) 195.
[33] J.C. Dyre, N.B. Olsen, T. Christensen, Phys. Rev. E 53 (1996) 2171.
[34] H. Bei, S. Shim, E.P. George, M.K. Miller, E.G. Herbert, G.M. Pharr, Scr. Mater. 57 (2007) 397–400.
[35] S. Scudino, K.B. Surreddi, G. Wang, J. Eckert, Scr. Mater. 62 (2010) 750–753.
[36] Z. Han, Y. Li, H.J. Gao, J. Mater. Res. 25 (2010) 1958–1962.